

Optics Letters

Efficient erbium-doped thin-film lithium niobate waveguide amplifiers

ZHAOXI CHEN,^{1,†} QING XU,^{2,†} KE ZHANG,¹ WING-HAN WONG,¹ DE-LONG ZHANG,^{2,3} EDWIN YUE-BUN PUN,¹ AND CHENG WANG^{1,*}

¹Department of Electrical Engineering & State Key Laboratory of Terahertz and Millimeter Waves, City University of Hong Kong, Kowloon, Hong Kong, China

²Department of Opto-electronics and Information Engineering, School of Precision Instruments and Opto-electronics Engineering, Key Laboratory of Optoelectronic Information Science & Technology (Ministry of Education), Tianjin University, Tianjin 300072, China

³e-mail: dlzhang@tju.edu.cn

*Corresponding author: cwang257@cityu.edu.hk

Received 20 January 2021; accepted 31 January 2021; posted 10 February 2021 (Doc. ID 420250); published 1 March 2021

Lithium niobate on insulator (LNOI) is an emerging photonic platform with great promise for use in future optical communications, nonlinear optics, and microwave photonics. An important integrated photonic building block, active waveguide amplifiers, however, are still missing in the LNOI platform. Here, we report an efficient and compact waveguide amplifier based on erbium-doped LNOI waveguides, achieved using a sequence of erbium-doped crystal growth, ion slicing, and lithography-based waveguide fabrication. Using a compact 5 mm long waveguide, we demonstrate an on-chip net gain of >5 dB for 1530 nm signal light with a relatively low pump power of 21 mW at 980 nm. The efficient LNOI waveguide amplifiers could become an important fundamental element in future lithium niobate photonic integrated circuits. © 2021 Optical Society of America

<https://doi.org/10.1364/OL.420250>

Lithium niobate on insulator (LNOI) has recently emerged as a promising material platform for compact, high-performance, and low-cost photonic circuits [1–3]. Compared to conventional bulk lithium niobate (LN) optical devices based on weakly confined waveguides, LNOI devices feature a smaller footprint, stronger optical confinement, and significantly higher nonlinear optical and electro-optic efficiencies. To date, a variety of high-performance LNOI devices have been achieved, including high-speed electro-optic modulators [4–7], efficient frequency convertors [8–11], frequency comb sources [12–14], photon-pair generators [15,16], as well as on-chip spectrometers [17]. However, an important functionality in photonic integrated circuits, namely active optical gain, is typically absent in the LNOI platform, limited by the material properties of intrinsic LN.

Doping LN crystals with erbium (Er) ions is a promising solution to achieve the missing optical gain function in the LNOI platform because Er³⁺ ions could provide significant gain near the telecom wavelength range, and the gain spectrum is not strongly affected by the host environment. In fact, Er-doping-based waveguide amplifiers have been used in many popular

integrated photonic platforms, including silicon nitride (SiN) [18,19], silicon (Si) [20], and other metal oxides [21]. In conventional bulk LN waveguides, Er-doped waveguide amplifiers have also been achieved, often by diffusing Er³⁺ ions into a titanium (Ti)-diffused channel or ridge waveguides [22,23]. Due to the weak optical confinement in these low-index-contrast waveguides ($\Delta n < 0.02$) and the diffusion-induced non-uniform Er³⁺ ion distribution, the optical net internal gain of bulk Er-doped LN (Er:LN) waveguide amplifiers are usually <3 dB/cm [24]. This approach, however, cannot be directly translated to the LNOI platform because the required diffusion temperature (>1100°C) is too high for the LN thin films due to thermal expansion and pyroelectric issues. One approach to achieve Er:LNOI wafers is to directly grow an Er:LN crystal, followed by a standard ion-slicing process to form the Er:LNOI wafer. Using this technique, microcavity-based Er:LNOI lasers have been demonstrated very recently, showing threshold powers below 1 mW [25–27]. An alternative approach is to perform ion implantation into LNOI wafers, although the implanted wafer still needs to go through certain annealing processes to activate the Er³⁺ ions, and the implantation concentration is relatively low so far [28].

In this Letter, we experimentally demonstrate an Er:LNOI waveguide amplifier with a high on-chip net gain of >10 dB/cm at a signal wavelength of 1531.6 nm. The lithography-defined waveguides feature strong light confinement for both 980 nm pump light and 1530 nm signal light. As a result, our devices could provide high gain at relatively low pump powers (<20 mW), and could yield efficient amplification within a large operational dynamic range (10 nW – 100 μ W signal power), with measured 980 to 1530 nm power conversion efficiencies up to 0.2%.

Fabrication of our Er:LNOI waveguide amplifiers starts from a bulk Z-cut LN wafer with an Er-doping concentration of ~0.5 mol% (OST Photonics). Doping of Er³⁺ ions is completed during the Czochralski growth of the LN crystal, as illustrated in Fig. 1(a). The Er:LN wafer appears as a rose-red color due to the fluorescence of Er³⁺ ions from ambient ultraviolet excitation [inset of Fig. 1(a)]. The bulk Er:LN wafer is then

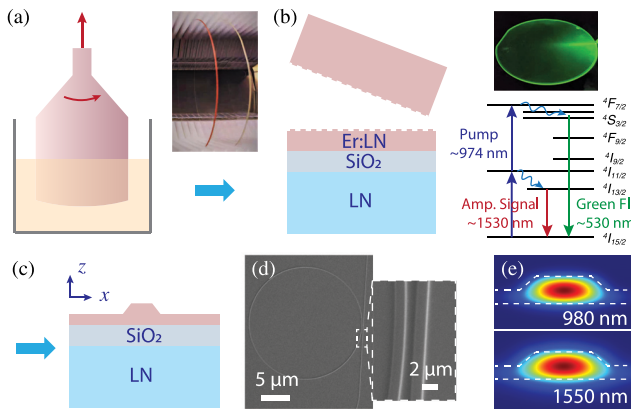


Fig. 1. (a) Czochralski process for Er:LN crystal growth. (b) Ion-slicing process to create Er:LNOI wafer. Inset: Er:LNOI wafer showing green fluorescence (top); Er^{3+} energy diagram (bottom). (c) Cross-section schematic of the final Er:LNOI rib waveguides. (d) SEM images of a waveguide-coupled Er:LN microring resonator. (e) Simulated electric field profiles (E_x) of TE_0 modes at 980 nm (top) and 1550 nm (bottom).

sent out for ion-slicing service (NANOLN), to transform into an Er:LNOI wafer with a top 700 nm thick Er:LN film, a 2 μm buried silica layer, and a 500 μm Z-cut un-doped LN bottom substrate, as shown in Fig. 1(b). When 980 nm laser light is shone from the edge, green fluorescence could be observed from the Er:LN thin film [insets of Fig. 1(b)]. To fabricate the optical waveguides, a 250 nm thick nichrome (NiCr) mask is first patterned through a sequence of electron-beam lithography (EBL), thermal evaporation, and standard lift-off processes. The mask patterns are subsequently transferred to the Er:LNOI layer by an argon (Ar^+)-based reactive ion etching (RIE) process. After removing the residual NiCr mask, a chemical-mechanical polishing (CMP) process is applied on the sample surface, which could typically further reduce the waveguide scattering loss by an order of magnitude [29,30]. The fabricated Er:LNOI waveguide has a rib-like structure, with a rib height of 320 nm, an un-etched slab thickness of 340 nm, a top width of 1.2 μm , and a sidewall angle of $\sim 45^\circ$ [Figs. 1(c)–1(e)]. Finally, the chip facets are carefully polished using a series of descending powder sizes to precisely control the total waveguide length (5 mm) and to produce smooth waveguide facets for efficient fiber-to-chip coupling. Figure 1(d) shows the scanning electron microscope (SEM) image of a waveguide-coupled microring resonator fabricated on the same chip as the waveguide amplifiers, revealing smooth-etched surfaces. The micron-scale waveguides support strong light confinement for both the 980 nm pump and 1530 nm signal light used in this work. Figure 1(e) shows the simulated field distributions (E_x) of the fundamental transverse-electric (TE) modes at both wavelengths.

We characterize the optical amplification performance of the fabricated Er:LNOI waveguides using an end-fire coupling system shown in Fig. 2(a). Pump light from a continuous-wave (CW) 980 nm laser source (Amonics ALD-980, actual output wavelength at 974.5 nm) and signal light from a CW telecom tunable laser (Santec TSL-550) are combined using a fiber-based wavelength-division multiplexer (WDM) and coupled into the Er:LNOI waveguides using a lensed fiber. In-line fiber polarization controllers are used to ensure TE polarization at

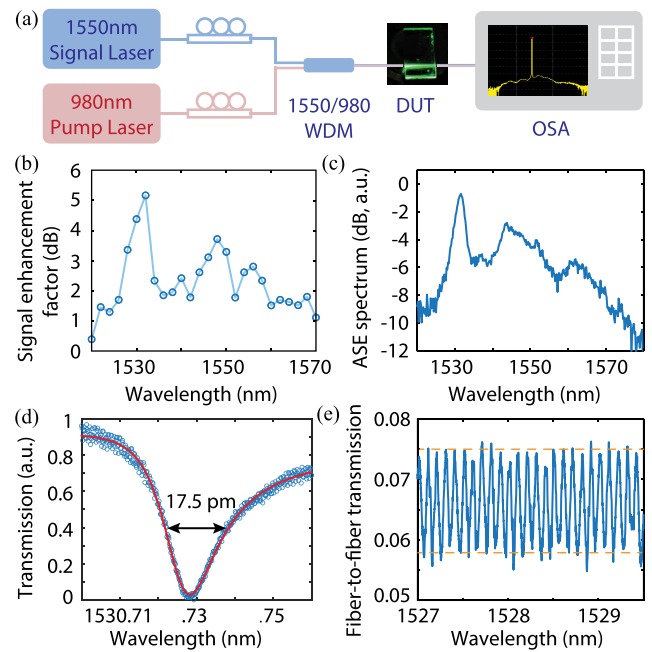


Fig. 2. (a) Experimental setup for gain characterization. (b) Signal enhancement factor versus signal wavelength. (c) ASE spectrum of the Er:LNOI waveguide. (d) Optical transmission spectrum (blue) and Fano-fit curve (red) of an Er:LNOI microring resonator. (e) Fiber-to-fiber transmission spectrum showing strong Fabry–Perot fringes.

the input, which shows the highest fiber-to-chip coupling efficiency in our devices. The output light is collected by a second lensed fiber and sent to an optical spectrum analyzer (OSA, YOKOGAWA AQ6370D). During our experiment processes, we observe strong up-conversion induced green photoluminescence along the tested Er:LNOI waveguides, as shown in the photograph in Fig. 2(a), indicating the Er^{3+} ions are well activated inside these etched structures.

We show that our Er:LNOI waveguides could provide signal amplification over the entire telecom C band [Fig. 2(b)]. To characterize the small-signal gain performance, we fix the input signal power at ~ 5 nW and measure the signal enhancement factor at various wavelengths, which is defined as the output signal power ratio between pump-on (~ 20 mW) and pump-off scenarios. The powers quoted here and after correspond to on-chip powers, where the fiber coupling losses have been calibrated out (details to be discussed later), and have a relative uncertainty value of around ± 0.12 dB. As Fig. 2(b) shows, the device features measurable signal amplification over the entire 1520–1570 nm range, with three enhancement peaks at ~ 1531 nm, 1546 nm, and 1554 nm. These peaks agree well with the amplified spontaneous emission (ASE) spectrum of our devices [Fig. 2(c)], measured when the signal laser is turned off, as well as the ASE spectrum in conventional Er-doped systems, strongly suggesting that the measured amplification phenomena in our devices are indeed the result of pump-induced Er^{3+} population inversion.

To further investigate the net internal gain of our Er:LNOI waveguide amplifiers, we perform a careful calibration of the waveguide loss at the signal wavelength using two corroborating measurements. We first characterize the quality (Q) factor of a microring resonator, fabricated on the same chip and with

similar dimensions as the Er:LNOI waveguides [Fig. 1(d)]. Figure 2(d) shows the optical transmission spectrum of a critically coupled resonance dip measured at 1530.73 nm. The resonance shows a slightly asymmetric line-shape due to the background Fabry–Perot interference pattern, which is induced by the reflections from the two polished chip facets. Nevertheless, the resonance spectrum can be fitted very well using a Fano function, revealing a resonance linewidth of 17.5 pm and an intrinsic Q factor of $Q_i = 176,000$. We can therefore estimate the propagation loss α of the tested Er:LNOI waveguides using the equation

$$\alpha = \frac{2\pi N_{\text{eff}}}{\lambda_0 Q_i}, \quad (1)$$

where N_{eff} is the effective index of the waveguide at the target wavelength λ_0 . The calculated propagation loss at 1530 nm is ~ 2 dB/cm. The second approach evaluates the waveguide loss using the contrast of the measured Fabry–Perot fringes [$\sim 13\%$ as shown in Fig. 2(e)] and the numerically simulated facet reflection coefficients [31], yielding an estimated propagation loss of 1.13 dB/cm. Considering the possible difference between the simulated and actual facet reflectivity, we take the conservative but more reliable loss estimate from the first approach (i.e., resonator Q -analysis) to avoid overestimation of the net gain, which leads to an on-chip loss of 1 dB for our 5 mm device. As such, the measured fiber-to-fiber insertion loss of ~ 12 dB [Fig. 2(e)] can be attributed to a 1 dB on-chip loss and an 11 dB coupling loss, the latter of which is consistent with previous reports on similar platforms [4]. We further estimate that approximately half of the 2 dB/cm propagation loss comes from the Er^{3+} ion absorption, since the measured Q factors in our un-doped LNOI microring resonators using the same fabrication method are typically $\sim 400,000$. The Er absorption loss at other telecom wavelengths should, in principle, be lower than that at 1530 nm, but the difference is too small to be resolved in our current measurements. In the rest of this Letter, we use a conservative 1 dB estimate of the internal loss for both 1530 nm and 1550 nm signal light.

Apart from the loss calibration at telecom wavelengths, we have also calibrated the coupling and propagation losses of our waveguides at 980 nm, by measuring and comparing the fiber-to-fiber insertion losses of the Er:LNOI waveguide and a short, un-doped LNOI waveguide with similar dimensions. The measured losses are 17 dB and 12 dB, respectively, indicating a 5 dB on-chip loss and a 6 dB/facet coupling loss at 980 nm. The launched pump and input/output signal powers in this Letter have been calibrated to the on-chip powers using the above measurement results.

We demonstrate strong net internal gain of >5 dB in our Er:LNOI waveguide amplifiers with a short device length and relatively low pump powers. Net internal gain is calculated by subtracting the internal loss from the measured signal amplification factor. Figure 3(a) shows the measured signal spectra at 1531.6 nm under a fixed signal power of 8.2 nW and increasing pump powers (0–21 mW). A maximum net internal gain of 5.2 dB is achieved at the highest pump power of 21 mW, corresponding to a net gain per unit length of >10 dB/cm, which is comparable with the gain achieved in other Er-doped integrated photonic systems [18–20]. When compared with typical bulk Er:LN waveguides (2–3 dB/cm) [22–24], our measured net internal gain is $\sim 5\times$ higher, likely due to the more efficient

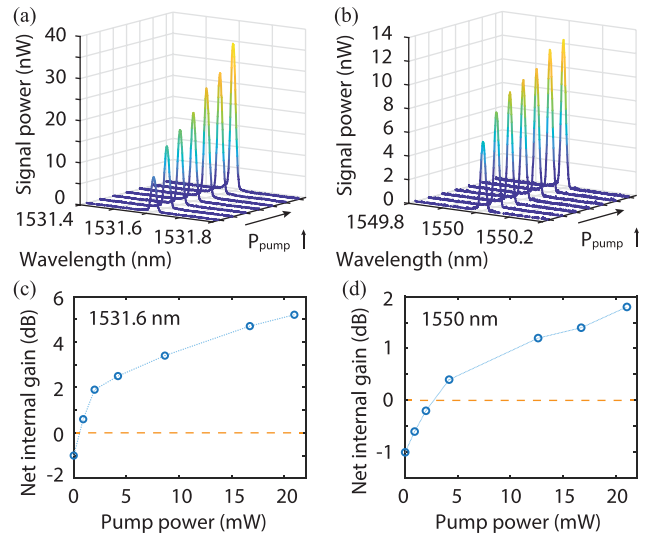


Fig. 3. (a), (b) Measured signal spectra as a function of increasing pump powers measured at (a) 1531.6 nm and (b) 1550 nm. Pump powers: 0, 1 mW, 2 mW, 4.2 mW, 8.6 mW, 16.7 mW, and 21 mW. (c), (d) Net internal gain as a function of pump power at (c) 1531.6 nm and (d) 1550 nm.

excitation and stimulated emission of Er^{3+} ions in these strongly confined waveguides. Figure 3(c) shows the measured net internal gain as a function of pump power. At small pump powers, the optical gain increases rapidly and becomes sufficient to compensate for the internal loss at pump powers <1 mW. The optical gain starts to see saturation behavior at pump powers >10 mW. We have also characterized the gain performance of our Er:LNOI waveguide amplifier at the signal wavelength of 1550 nm (signal power = 5.8 nW). As shown in Figs. 3(b) and 3(d), similar signal amplification phenomena could be observed at 1550 nm, but with lower gain than 1531.6 nm. A maximum net internal gain of 1.8 dB is achieved at a pump power of 21 mW, corresponding to a net gain per unit length of 3.6 dB/cm. Further reducing the waveguide scattering loss by optimizing the fabrication process could potentially improve the net gain by another 1 dB/cm.

We further characterize the operation dynamic range of our Er:LNOI waveguide amplifier by increasing the signal power until the system reaches the saturated-gain regime. With a fixed pump power of 21 mW, the net internal gain gradually drops with increasing signal power, from the small-signal value of ~ 5 dB to a final value of 0.5 dB at -10 dBm signal, as is shown in Fig. 4(a). Considering the internal loss of 1 dB, the 0.5 dB net internal gain still corresponds to a significant power amplification ($\sim 40\%$ increase from a pump-off scenario), indicating a signal power dynamic range of at least 50 dB. Using these data, we estimate the internal conversion efficiency η of our Er:LNOI amplifier, which is defined as

$$\eta = 100\% \times (P_{\text{signal,on}} - P_{\text{signal,off}}) / P_{\text{pump}}, \quad (2)$$

where P_{pump} is the launched pump power, and $P_{\text{signal,on}}$ and $P_{\text{signal,off}}$ are the output signal powers with and without pump light injection, respectively. Note that η here corresponds to the nominal gain rather than net gain, since the generated power for compensating the initial internal loss is also converted from 980 nm by the Er^{3+} ions. As Fig. 4(b) shows, the measured

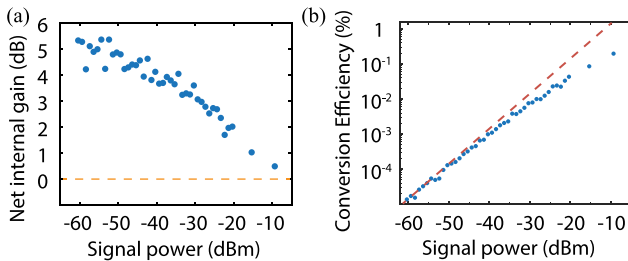


Fig. 4. (a) Dependence of net internal gain on signal power. (b) Measured internal conversion efficiency (blue dots) as a function of signal power. Red-dashed line shows the linear trend according to small-signal gain.

conversion efficiency increases linearly with the signal power in the small-signal regime, then gradually deviates from the linear trend since the excited-state Er^{3+} ions are consumed substantially by the signal light in the saturated-gain regime. At the maximum signal power of $100 \mu\text{W}$, the internal conversion efficiency achieves a value of 0.2%, which is not yet fully saturated. We expect the saturated conversion efficiency in our current devices to be $\sim 1\%$. The conversion efficiency as well as signal amplification performance could potentially be further improved in future work by increasing the Er^{3+} doping concentration, optimizing the pump wavelength and device length, as well as using improved waveguide designs.

In conclusion, we have demonstrated an Er:LNOI waveguide amplifier with maximum net internal gain of 5.2 dB achieved in a 5 mm long device. During the preparation of this Letter, we noted that a similar Er:LNOI waveguide amplifier work was posted as an arXiv preprint [32], where the authors have demonstrated similar amplification results using a different waveguide fabrication approach. Our efficient and compact waveguide amplifiers could provide solutions for a long-awaited missing piece, active gain elements, in the LNOI photonic platform. Combining them with existing passive LNOI elements on the same chip, e.g., by selective-area pumping or doping, could enable a variety of loss-sensitive applications in optical communications and microwave photonics. The added gain functionality could also provide new functional degrees of freedom that could enable novel photonic systems such as parity-time symmetric systems.

Funding. National Natural Science Foundation of China (61922092, 61875148); Research Grants Council, University Grants Committee (CityU 11210317, CityU 21208219); City University of Hong Kong (9610402, 9610455).

Disclosures. The authors declare no conflicts of interest.

Data availability. Data underlying the results presented in this paper are not publicly available at this time but may be obtained from the authors upon reasonable request.

[†]These authors contributed equally to this Letter.

REFERENCES

- A. Boes, B. Corcoran, L. Chang, J. Bowers, and A. Mitchell, *Laser Photon. Rev.* **12**, 1700256 (2018).
- J. Lin, F. Bo, Y. Cheng, and J. Xu, *Photon. Res.* **8**, 1910 (2020).
- A. Rao and S. Fathpour, *IEEE J. Sel. Top. Quantum Electron.* **24**, 8200912 (2018).
- C. Wang, M. Zhang, X. Chen, M. Bertrand, A. Shams-Ansari, S. Chandrasekhar, P. Winzer, and M. Lončar, *Nature* **562**, 101 (2018).
- M. Xu, M. He, H. Zhang, J. Jian, Y. Pan, X. Liu, L. Chen, X. Meng, H. Chen, Z. Li, X. Xiao, S. Yu, S. Yu, and X. Cai, *Nat. Commun.* **11**, 3911 (2020).
- B. Pan, J. Hu, Y. Huang, L. Song, J. Wang, P. Chen, L. Liu, and D. Dai, in *Asia Communications and Photonics Conference* (Optical Society of America, 2020), paper M4D.7.
- M. Li, J. Ling, Y. He, U. A. Javid, S. Xue, and Q. Lin, *Nat. Commun.* **11**, 4123 (2020).
- S. Liu, Y. Zheng, Z. Fang, X. Ye, Y. Cheng, and X. Chen, *Opt. Lett.* **44**, 1456 (2019).
- C. Wang, C. Langrock, A. Marandi, M. Jankowski, M. Zhang, B. Desiatov, M. M. Fejer, and M. Lončar, *Optica* **5**, 1438 (2018).
- J. Lu, J. B. Surya, X. Liu, A. W. Bruch, Z. Gong, Y. Xu, and H. X. Tang, *Optica* **6**, 1455 (2019).
- J. Y. Chen, Z. H. Ma, Y. M. Sua, Z. Li, C. Tang, and Y. P. Huang, *Optica* **6**, 1244 (2019).
- C. Wang, M. Zhang, M. Yu, R. Zhu, H. Hu, and M. Loncar, *Nat. Commun.* **10**, 978 (2019).
- M. Zhang, B. Buscaino, C. Wang, A. Shams-Ansari, C. Reimer, R. Zhu, J. M. Kahn, and M. Lončar, *Nature* **568**, 373 (2019).
- Y. He, Q. Yang, J. Ling, R. Luo, H. Liang, M. Li, B. Shen, H. Wang, K. Vahala, and Q. Lin, *Optica* **6**, 1138 (2019).
- J. Zhao, C. Ma, M. Rüsing, and S. Mookherjee, *Phys. Rev. Lett.* **124**, 163603 (2020).
- B. S. Elkus, K. Abdelsalam, A. Rao, V. Veleev, S. Fathpour, P. Kumar, and G. S. Kanter, *Opt. Express* **27**, 38521 (2019).
- D. Pohl, M. Reig Escalé, M. Madi, F. Kaufmann, P. Brotzer, A. Sergeev, B. Guldemann, P. Giaccari, E. Alberti, U. Meier, and R. Grange, *Nat. Photonics* **14**, 24 (2020).
- H. C. Frankis, H. M. Mbonde, D. B. Bonneville, C. Zhang, R. Mateman, A. Leinse, and J. D. B. Bradley, *Photon. Res.* **8**, 1022 (2020).
- J. Rönn, W. Zhang, A. Autere, X. Leroux, L. Pakarinen, C. Alonso-Ramos, A. Säynätjoki, H. Lipsanen, L. Vivien, E. Cassan, and Z. Sun, *Nat. Commun.* **10**, 432 (2019).
- S. A. Vázquez-Córdova, M. Dijkstra, E. H. Bernhardt, F. Ay, K. Wörhoff, J. L. Herek, S. M. García-Blanco, and M. Pollnau, *Opt. Express* **22**, 25993 (2014).
- A. Z. Subramanian, G. S. Murugan, M. N. Zervas, and J. S. Wilkinson, *Opt. Commun.* **285**, 124 (2012).
- D. Brüske, S. Suntsov, C. E. Rüter, and D. Kip, *Opt. Express* **25**, 29374 (2017).
- D. Zhang, F. Han, B. Chen, P. Hua, D. Yu, and E. Y. B. Pun, *J. Lightwave Technol.* **32**, 135 (2014).
- J. D. B. Bradley and M. Pollnau, *Laser Photon. Rev.* **5**, 368 (2011).
- Z. Wang, Z. Fang, Z. Liu, W. Chu, Y. Zhou, J. Zhang, R. Wu, M. Wang, T. Lu, and Y. Cheng, *Opt. Lett.* **46**, 380 (2021).
- Y. Liu, X. Yan, J. Wu, B. Zhu, Y. Chen, and X. Chen, *Sci. China Phys. Mech. Astron.* **64**, 234262 (2021).
- Q. Luo, Z. Z. Hao, C. Yang, R. Zhang, D. H. Zheng, S. G. Liu, H. De Liu, F. Bo, Y. F. Kong, G. Q. Zhang, and J. J. Xu, *Sci. China Phys. Mech. Astron.* **64**, 234263 (2021).
- S. Wang, L. Yang, R. Cheng, Y. Xu, M. Shen, R. L. Cone, C. W. Thiel, and H. X. Tang, *Appl. Phys. Lett.* **116**, 151103 (2020).
- M. Wang, R. Wu, J. Lin, J. Zhang, Z. Fang, Z. Chai, and Y. Cheng, *Quantum Eng.* **1**, e9 (2019).
- R. Wolf, I. Breunig, H. Zappe, and K. Buse, *Opt. Express* **26**, 19815 (2018).
- D. Hofstetter and R. L. Thornton, *Opt. Lett.* **22**, 1831 (1997).
- J. Zhou, Y. Liang, Z. Liu, W. Chu, H. Zhang, D. Yin, Z. Fang, R. Wu, J. Zhang, W. Chen, Z. Wang, Y. Zhou, M. Wang, and Y. Cheng, "On-chip integrated waveguide amplifiers on Erbium-doped thin film lithium niobate on insulator," arXiv:2101.00783 (2021).